Brain Structure and Function
https://doi.org/10.1007/s00429-023-02681-4

ORIGINAL ARTICLE

Early development of the functional brain network in newborns

Reza Nazari[1] · **Mostafa Salehi**[1,2]

Received: 24 December 2022 / Accepted: 6 July 2023

Abstract
During the prenatal period and the first postnatal years, the human brain undergoes rapid growth, which establishes a preliminary infrastructure for the subsequent development of cognition and behavior. To understand the underlying processes of brain functioning and identify potential sources of developmental disorders, it is essential to uncover the developmental rules that govern this critical period. In this study, graph theory modeling and network science analysis were employed to investigate the impact of age, gender, weight, and typical and atypical development on brain development. Local and global topologies of functional connectomes obtained from rs-fMRI data were collected from 421 neonates aged between 31 and 45 postmenstrual weeks who were in natural sleep without any sedation. The results showed that global efficiency, local efficiency, clustering coefficient, and small-worldness increased with age, while modularity and characteristic path length decreased with age. The normalized rich-club coefficient displayed a U-shaped pattern during development. The study also examined the global and local impacts of gender, weight, and group differences between typical and atypical cases. The findings presented some new insights into the maturation of functional brain networks and their relationship with cognitive development and neurodevelopmental disorders.

Keywords Functional connectivity · Brain network · Early brain development · Network science · Graph theory · Resting state fMRI

Introduction

The human brain undergoes profound anatomical and functional transformations during early development, particularly from the last trimester of pregnancy through the first two postnatal years (Knickmeyer et al. 2008; Gilmore et al. 2018; Kostović et al. 2019; Li et al. 2019). These changes lay the foundation for later behavioral and cognitive progressions and facilitate the acquisition of fundamental skills during subsequent years (Yakovlev 1967; Huttenlocher 1979; Huttenlocher and Dabholkar 1997; Miller et al. 2012). Furthermore, several major psychiatric disorders can significantly disrupt the typical sequence of development during early brain development (Marín 2016; Hazlett et al. 2017). Therefore, it is imperative to recognize both typical and atypical developmental changes in the brain's topological features to identify developmental disorders at an early stage.

It is essential to comprehend the development of various interlinked brain systems in addition to studying the maturation of structural and functional aspects across different brain regions. Advanced non-invasive imaging techniques have facilitated researchers in mapping the structural and functional connectivity of the brain network and identifying the reorganization of neural interactions within a network framework (Kelly et al. 2012; Sporns 2013; Salehi et al. 2010; Cao et al. 2017; Centeno et al. 2022). The use of network science in functional brain networks has shown key topological characteristics impacting human behavior, such as the efficient network architecture, the small-world topology (Onoda and Yamaguchi 2013; John et al. 2017; Päeske et al. 2020), which maintains a balance of integration and segregation for fast information transfer between the areas, the modular structure (Onoda and Yamaguchi 2013; Boeken et al. 2022), the high-central or high-degree hubs (Markett et al. 2016; Chen et al. 2021; Neudorf et al. 2022), and the

✉ Mostafa Salehi
mostafa_salehi@ut.ac.ir

[1] Faculty of New Sciences and Technologies, University of Tehran, Tehran, Iran

[2] School of Computer Science, Institute for Research in Fundamental Science (IPM), Tehran, P.O.Box 19395-5746, Iran

Published online: 26 July 2023

rich-club architecture (van den Heuvel and Sporns 2013; Kim and Min 2020; Zhao et al. 2021), which is comprised highly interconnected hubs forming the main backbone for the network's efficient communication.

Research on the functional brain networks of infants has uncovered significant changes in early topological properties. Studies have shown that the infant brain network undergoes continuous reorganization, with only a few connections rewired to establish more efficient organizations (Thomason et al. 2015; Cao et al. 2017; Zhao et al. 2019). These changes in functional interactions mediate the emergence of complex cognitive functions in the early stages after childbirth (Cohen and D'Esposito 2016). Previous investigations of functional connectivity, utilizing independent component analyses or seed-based connectivity, have detected distinctive functional networks in the infant brain, including primary auditory, visual, and sensorimotor networks, as well as the default-mode and executive-control networks engaged in heteromodal tasks (Thomason et al. 2015; Gao et al. 2015; Emerson et al. 2016; Rajasilta et al. 2020).

Additionally, network science showed that small-world property and rich-club organization were discovered in the brains of premature neonates at around 30 postmenstrual weeks (PMW) (Cao et al. 2017). Hubs in mature newborns spread into the visual and primary sensorimotor regions as well as the Wernicke's region as they develop (Fransson et al. 2011; Cao et al. 2017). A remarkable modular structure was detected in fetal brains during the gestational age of about 20 weeks in utero (Thomason et al. 2014), and in preterm brains at around 30 postmenstrual weeks (Cao et al. 2017). Moreover, the functional networks' clustering coefficient significantly increased, and their participation coefficient decreased with age (Cao et al. 2017). This indicates an increased segregation process happening during development. In the fetal fMRI study (Thomason et al. 2014), findings also revealed a decrease in modularity and an increase in the strength of connections between the modules with age, indicating an improvement in the network integration process. After childbirth, the local and global efficiencies of the functional connectomes increased in one-year-old infants compared with neonates, but remained unchanged in the second year (Gao et al. 2011). Following the first year of life, one MEG study identified significant increases in the sensorimotor network's global and local efficiencies (Berchicci et al. 2015). These changes refer to an enhancement in both network segregation and integration processes during the early postnatal period.

Investigating the brain at an earlier stage than full-term birth is of paramount importance for comprehending the emergence of topological properties in brain networks. However, previous studies have primarily utilized adult preprocessing pipelines and structural atlases, focused on a limited number of network metrics, employed cross-sectional analyses, and utilized small sample sizes. Therefore, it is crucial to employ more advanced and comprehensive techniques on high-quality data to investigate the early developmental trajectory of the neonatal brain. Due to the unique characteristics of neonatal brains and the differences in data acquisition, anatomy, tissue composition, low contrast, and high levels of head motion, it is necessary to utilize a different framework to preprocess fMRI data (Cusack et al. 2017; Mongerson et al. 2017; Smyser et al. 2016). This study utilized the dHCP neonatal fMRI pipeline (Fitzgibbon et al. 2020), which minimally preprocesses the data with high-quality assurance and low failure rates. Additionally, we regressed out the average white matter (WM) and cerebrospinal fluid (CSF) signals from the voxels' time series, and the resulting images were subjected to bandpass filtering and smoothing (Salimi-Khorshidi et al. 2014; Howell et al. 2020). In the network construction step, we aimed to capture functional connectivity patterns and ensure more information retention and an accurate representation of the connectivity between different brain regions in this population (Craddock et al. 2012; Shi et al. 2018; McGrath et al. 2022). To achieve this, we defined the network nodes using the functional neonatal atlas and employed weighted edges to enhance information retention between the network nodes, thus generating homogeneous functional brain regions and functional connectivity patterns. Prior infant research has predominantly focused on the impact of age, and there is evidence suggesting significant gender differences in the network properties of structural and functional brain networks in adults (Smith et al. 2014; Mijalkov et al. 2023). Therefore, in this study, our objective was to examine broader factors, including the impact of age, weight, gender, and typical and atypical development, as well as their interactions, on the network metrics from 31 to 45 postmenstrual weeks. We explored various functional network metrics, such as global efficiency, local efficiency, node degree, normalized rich-club coefficient, modularity, clustering coefficient, small-worldness, and characteristic path length. Based on previous studies, we expected that the functional network of typical neonates would exhibit increased global and local efficiency (Gao et al. 2011; Berchicci et al. 2015) and decreased modularity (Thomason et al. 2014) with age. Additionally, we hypothesized that age, weight, gender, and group differences between typical and atypical cases would impact the functional connectome's local and global topological characteristics. By employing a network science approach, we conducted a comprehensive analysis of the whole-brain functional network topology to identify differences in network metrics between typical and atypical participants and among males and females with varying weights.

Materials and methods

Participants and MR acquisition

The subjects of this study were four hundred and twenty-one ($N = 421$) healthy neonates aged between 31 and 45 weeks of gestation. As a part of the Developing Human Connectome Project (dHCP), the third data release (2021), their MR images were scanned. They were 225 males and 196 females, among which 363 neonates were typical and 58 were atypical (DHCP 2021). It is necessary to note that the third open-access data release comprised the images of 783 neonatal participants. All newborns underwent one 63-minute scanning session on a three Tesla medical scanner equipped with a 32-channel dedicated neonatal head coil (Hughes et al. 2017). The data included structural imaging, diffusion magnetic resonance imaging (dMRI), and resting-state functional magnetic resonance imaging (rs-fMRI). The structural MR images had high resolution, i.e., T1-weighted and T2-weighted images, with an in-plane resolution of $0.8 \times 0.8\ mm^2$ and a thickness of 1.6 *mm* overlapped by 0.8 *mm* (Hughes et al. 2017; Cordero-Grande et al. 2018). A high-temporal resolution multiband EPI sequence ($TR = 392\ ms$; 2.15 *mm* isotropic) was used to obtain approximate 15 *min* (2300 volumes) of rs-fMRIs from each participant. Additionally, single-band EPI reference scans were gathered with a bandwidth-matched readout, followed by spin echo EPI acquisitions with PA (posterior → anterior) and AP (anterior → posterior) phase-encoding directions (Malik 2015; Price et al. 2015).

This data release had some minimal accompanying metadata, such as age at birth, age at scan, gender, birth weight, head circumference, and the radiology score (radScore). A specialist in perinatal neuroradiology examined the MRI scans using the radiology score, implementing the following scales (DHCP 2021): 1 = normal appearance for age; 2 = incidental findings with some trivial significance for the clinical outcome or analysis, like the subdural hemorrhage, isolated subependymal cysts, and mild inferior vermis rotation; 3 = incidental results with trivial clinical significance but conceivable analytical significance, such as the existence of several punctate lesions or some other focal white matter or cortical lesions that were not of clinical significance; 4 = incidental results with conceivable clinical significance and unseeming analytical significance, like the isolated non-brain anomaly in the pituitary or on the tongue; 5 = incidental results with conceivable significance for the clinical and imaging analyses, such as the detection of important lesions in the white matter cortex, the cerebellum, and/or the basal ganglia, as well as the small head or brain, i.e., < 1 st centile; Q = poor-quality data. The present study implemented radScore = 1 and radScore = 5 to represent typical and atypical cases, respectively. Table 1 presents a comprehensive overview of the demographic information.

Preprocessing and network construction

Figure 1 displays the multi-threshold functional processing pipeline that was implemented to construct and analyze the functional brain networks of the neonates. The pipeline utilized several Python packages, including `ANTsPy` (Avants et al. 2009), `fslpy` (Jenkinson et al. 2012; Smith et al. 2004), `pybids` (Gorgolewski et al. 2016), `nilearn` (Abraham et al. 2014), and the `Brain Connectivity Toolbox for Python (BCTPY)` (Rubinov and Sporns 2010). In addition, statistical analysis was performed using the `statsmodels` (Seabold and Perktold 2010) package.

The T2-weighted images were analyzed using the dHCP preprocessing pipeline as the anatomical reference to provide a solid contrast for brain tissue segmentation compared to the T1-weighted images (Bozek et al. 2018; Makropoulos et al. 2018). Bias correction was implemented in the preprocessing procedure using the N4 algorithm (Tustison et al. 2010), followed by brain extraction using FSL-BET (Brain Extraction Tool) (Jenkinson et al. 2012; Smith 2002). The DRAW-EM algorithm was then used to segment the images into gray matter (GM), white matter (WM), and cerebrospinal fluid (CSF) (Makropoulos et al. 2014).

The dHCP preprocessing pipeline was also utilized for the minimally preprocessed rs-fMRI data. This procedure involved correcting susceptibility field distortions, the timing of slices, and motion artifacts (Fitzgibbon et al. 2020). Additionally, images were denoised by removing motion artifacts, followed by independent component analysis (ICA) and high-pass filtering (150 *s*) using FSL-FIX (Salimi-Khorshidi et al. 2014). The images were then transformed to the T2-weighted space and further into the newborn's standard template space (Fitzgibbon et al. 2020; Serag et al. 2012). The average WM and CSF signals from the voxels' time series were regressed out

Table 1 Demographic information of the participants in this study

Group	*N*	Male,	Birth age (weeks)		Scan age (weeks)		Birth weight (kg)
		N (%)	Mean±SD	Range	Mean±SD	Range	Mean±SD
Typical	363	197 (54)	38.3±3.5	23.7−42.7	40.6±2.8	32.1−44.9	3.0±0.8
Atypical	58	28 (48)	34.1±5.1	23.0−42.1	38.6±3.6	31.4−44.3	2.2±1.0

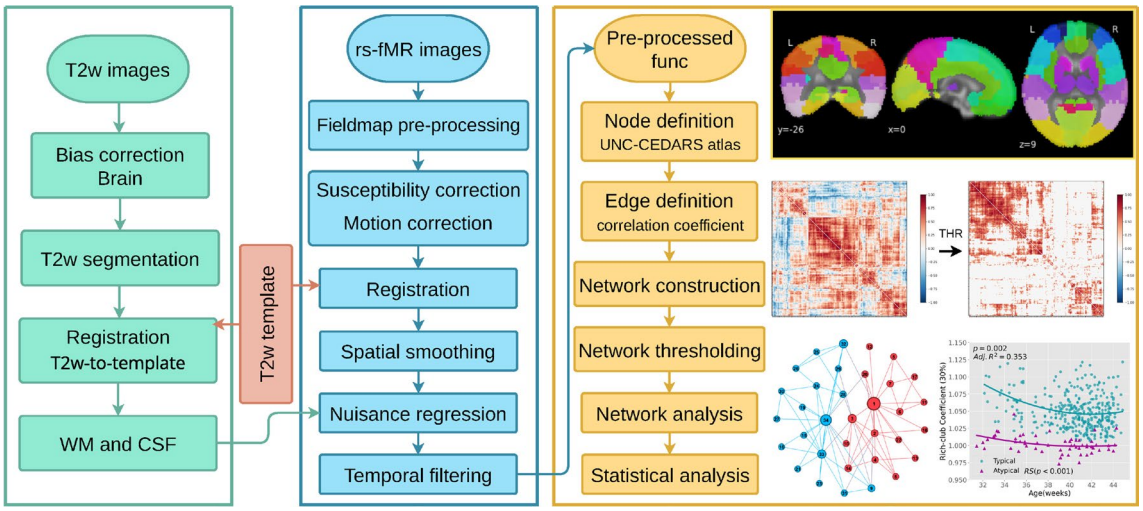

Fig. 1 Multi-threshold functional processing pipeline used for the construction and analysis of neonatal functional connectomes. The sMRI and fMRI images underwent minimal preprocessing using the dHCP preprocessing pipeline. Additionally, the average WM and CSF signals from the voxels' time series were regressed out, and the resulting images were subjected to bandpass filtering and smoothing. The network nodes were defined using the functional neonatal atlas, and weighted edges were computed between each pair of nodes using Pearson's correlation. The derived functional connectivity matrices were then thresholded, and network properties were calculated. Finally, statistical analysis was conducted to ascertain the changes in the functional network topology, assessing the impacts of age, weight, gender, and radiology score

in addition to the minimal preprocessing steps. The resulting images were bandpass filtered in the frequency range of $0.009 - 0.08Hz$ and smoothed with a 3 *mm* FWHM Gaussian kernel, as recommended by Howell et al. (2020) (see Fig. 1).

Defining the nodes of a network is a crucial step in applying network science methods to functional brain data. Although some infant studies have used anatomical atlases as nodes (Gao et al. 2011; Asis-Cruz et al. 2015), these atlases have limitations in terms of functional homogeneity and representation of functional connectivity patterns (Craddock et al. 2012; Shi et al. 2018). To generate homogeneous functional regions of interest (ROIs), the entire brain was parcellated into 223 cortical and subcortical nodes, utilizing the functional neonatal atlas provided by Shi et al. (2018). The atlas was warped back to its native space for each participant using the inverted deformation field derived from the registration step. Subsequently, the average time courses of all voxels within each ROI were extracted, and Pearson's correlation was computed between each pair of nodes, resulting in a 223×223 pairwise connectivity matrix for each subject. Different thresholding approaches were used to ensure that the findings were not biased by a single threshold. Furthermore, the derived functional connectivity matrices were thresholded into various densities ranging from 10% to 50% in 10% increments, yielding weighted functional connectivity networks at each density setting. The density range was determined by what was commonly used in the existing literature, where the network science analysis was performed (Cao et al. 2019). The absolute thresholding approach was also employed to conduct additional evaluations. Since the anti-correlations were still biologically unclear (Garrison et al. 2015), the positive connections were retained, and all negative values were set to zero. Ultimately, six weighted connectivity matrices were obtained for each participant.

Functional network analysis

The network properties were calculated using the `Brain Connectivity Toolbox for Python, version 0.5.2` (Rubinov and Sporns 2010). The functional connectivity matrices obtained for each participant were processed by the toolbox to quantify the topological properties of the functional connectomes, including global efficiency, local efficiency, node degree, normalized rich-club coefficient, modularity, clustering coefficient, small-worldness, and characteristic path length. To calculate the normalized rich-club coefficient, normalized clustering coefficient, and normalized characteristic path length, the $M = 1000$ random networks were used, while maintaining the network's degree and strength distributions. The network properties are given as follows:

Node degree is defined as one of the most important properties of a brain network and is represented as k. It is the number of edges attaching to a node in the network showing the local complexity of the network at the node (Bullmore and Sporns 2009).

According to Watts and Strogatz (1998), the node clustering coefficient is the one quantifying the tendency of pairs of nodes to be interconnected with each other if they are

connected to another node. The clustering coefficient C of a network G is defined as the average of the clustering coefficient over all nodes. It is calculated as follows,

$$C = \frac{1}{N}\sum_{i=1}^{N}\frac{\Gamma_i}{k_i(k_i-1)} \tag{1}$$

where, Γ_i is edges between the neighbors and N is the node numbers.

A path shows a route of edges connecting one node with the other nodes. Its length is the sum of the edges' numbers or weights. Here, the shortest path in a network between the two nodes is a path with minimum sum of the edge weights. As Bullmore and Sporns (2009) argues the characteristic path length L, shows the average shortest path length between all the feasible pairs of nodes and is defined as,

$$L = \frac{1}{N(N-1)}\sum_{1\le i,j\le N, i\ne j} l_{ij} \tag{2}$$

where, N is the number of nodes and l_{ij} is the shortest path length between nodes i and j.

As Latora and Marchiori (2001) argue, the ability of parallel information exchanges through the network is measured by global efficiency. It is the average of the inverse of the shortest path length between all pairs of nodes and is given as,

$$E(G) = \frac{1}{N(N-1)}\sum_{1\le i,j\le N, i\ne j}\frac{1}{l_{ij}} \tag{3}$$

where, N is the network's G number of nodes and l_{ij} is the shortest path length between the node i and the node j.

Local efficiency shows the capacity of the network's fault tolerance. It also displays the capacity to transfer information within the neighbors of a particular node (Latora and Marchiori 2001). Local efficiency is the global efficiency average of each node's neighborhood subgraph:

$$E_{loc}(G) = \frac{1}{N}\sum_{i=1}^{N} E(G_i) \tag{4}$$

where, G_i denotes the subgraph comprising all nodes of the immediate neighbors of node i.

Modularity refers to the degree of the network splitting up into a subpart with a higher connection with each other compared with the network's other parts (Newman 2006).

Small-world networks have numerous short-range connections with a few long-range ones. To investigate the small-worldness properties of a network, the normalized clustering coefficient and normalized characteristic path length are calculated (Watts and Strogatz 1998). The clustering coefficient and the characteristic path length of a network are C and L respectively, while the mean clustering coefficient and the mean characteristic path length of the M matched random networks are C_{rand} and L_{rand}. To check if a network is a small-world network, the following criteria are used: $\gamma = C/C_{\text{rand}} > 1$, and $\lambda = L/L_{\text{rand}} \approx 1$; Thus, $\sigma = \gamma/\lambda > 1$.

When the hub nodes like to be more interconnected with one another than by a random chance, we have rich-club organization (Van Den Heuvel and Sporns 2011), and the weighted rich-club coefficient is given as,

$$\phi^W(r) = \frac{W_{>r}}{\sum_{i=1}^{E_{>r}} w_i^{\text{rank}}} \tag{5}$$

where, $W_{>r}$ is the total of weights on the edges in the subgraph of nodes with rank greater than r, $E_{>r}$ is the number of edges in this subgraph, and w^{rank} is a vector of all edge weights, ranked from the largest to the smallest weight (Opsahl et al. 2008). The rich-club coefficient should be compared to an ensemble of randomized surrogate graphs to calculate a normalized rich-club coefficient, $\phi^W_{\text{norm}}(r) = \phi^W(r)/\phi^W_{\text{rand}}(r)$. where, $\phi^W_{\text{rand}}(r)$ is the average rich-club coefficient over M random networks (Alstott et al. 2014).

Statistical analysis

To ascertain the changes in the functional connectomes during the developmental period, a general linear model (GLM) was used to analyze the impacts of age, weight, gender, and radiology score (radScore) and their interactions with the network metrics. Multiple linear regressions were performed, including *age* and age^2 as predictors, as well as *weight*, *gender*, and *radScore* as the other covariates. In order to account for potential nonlinear patterns, the independent variable age^2 was included to assess quadratic developmental trajectories. So the following GLM models were considered:

$$Y_1 = \beta_0 + \beta_1\ \text{age} + \beta_2\ \text{weight} + \beta_3\ \text{gender} + \beta_4\ \text{radScore} \tag{6}$$

$$Y_2 = \beta_0 + \beta_1\ \text{age} + \beta_2\ \text{age}^2 + \beta_3\ \text{weight} + \beta_4\ \text{gender} + \beta_5\ \text{radScore} \tag{7}$$

To investigate the differences related to radiology scores and their developments, other GLM model with *age*, age^2, *weight*, *radScore* and radScore-by-age interactions was used. It examined both positive (typical > atypical) and negative (atypical > typical) contrasts, and the positive and negative age-by-radScore interactions.

$$\begin{aligned} Y_3 = {} & \beta_0 + \beta_1\ \text{age} + \beta_2\ \text{age}^2 + \beta_3\ \text{weight} \\ & + \beta_4\ \text{radScore} + \beta_5\ \text{radScore age} \end{aligned} \tag{8}$$

To analyze the differences related to threshold, a multiple linear regression Y3 on multiple thresholds for each network property was applied to model the effects of age, weight, gender, and their interactions. The statistical analyses were all carried out using Python and the `statsmodels package, version 0.13.2` (Seabold and Perktold 2010).

Results

During development, the functional network topology of the neonatal brains showed a significant correlation with age ($p < 0.05$). The developmental trajectories of important network properties from 31 to 45 weeks of age are presented in Figures 2, 3, 4, 5, 6. Positive age-related changes were observed in global efficiency (Fig. 2), local efficiency (Fig. 3), clustering coefficient (Fig. 5b), and small-worldness (Fig. 5c). Conversely, negative age-related changes were noted in modularity (Fig. 6) and characteristic path length (Fig. 5a), while the normalized rich-club coefficient (Fig. 4) displayed a positive quadratic trend.

Statistically significant radScore differences ($p < 0.05$) were found in the global efficiency (Fig. 2), local efficiency (Fig. 3), normalized rich-club coefficient (Fig. 4), and clustering coefficient (Fig. 5b) between typical and atypical subjects. Specifically, the typical group exhibited significantly higher values than the atypical group. Furthermore, there were significant radScore differences ($p < 0.05$) in the characteristic path length (Fig. 5a), with the atypical subjects having a higher value compared to the typical subjects. However, there were no significant radScore differences in the network modularity between the two groups.

Significant weight differences ($p < 0.05$) were observed in the global efficiency (Fig. 2), local efficiency (Fig. 3), normalized rich-club coefficient (Fig. 4), characteristic path length (Fig. 5a) and clustering coefficient (Fig. 5b). However, no significant gender differences were found in any of the network metrics at various thresholds. considering all values across multiple thresholds, males exhibited higher values of modularity (Fig. 7d) and the normalized rich-club coefficient (Fig. 7c) compared to females ($p < 0.05$).

To identify the regions with the highest connections within a functional brain network, the degree metric was used to detect hub nodes across all participants. The network hubs were identified as nodes with high degrees ($k >$ Mean + 1.5 SD). Our findings indicate that the predominant network hubs are situated in PreCG-L, MFG, SFGmed, ACG-R, MCG, PCUN-R, and MTG (see Table 2).

Furthermore, the rich-club organization was observed in the brain's topology because the hub nodes were more densely interconnected compared to other brain regions. The normalized rich-club coefficient showed a decreasing trend followed by an increasing trend during the neonatal period ($p < 0.05$) with considerable variability between 31 and 45 weeks across all different thresholds (refer to Fig. 4).

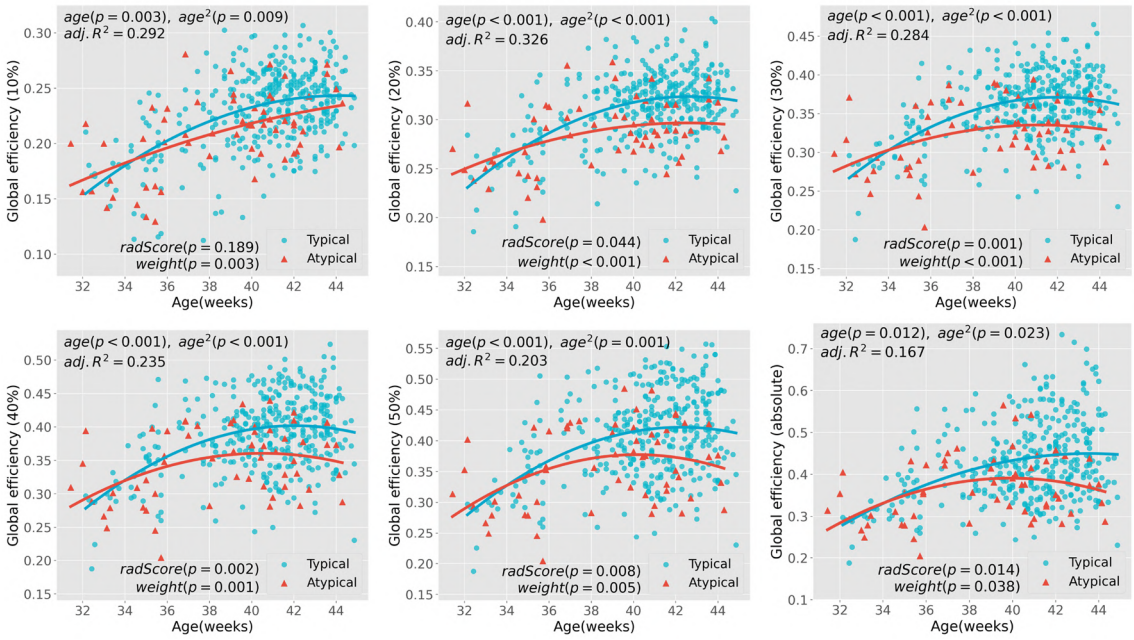

Fig. 2 Global efficiency values as a function of age and radScore differences across various thresholds. The plots illustrate the regression line for global efficiency values from 31 to 45 postmenstrual weeks of age. The $adj.R^2$ values were calculated using *age* and age^2 as predictors, and *weight* and *radScore* as other covariates

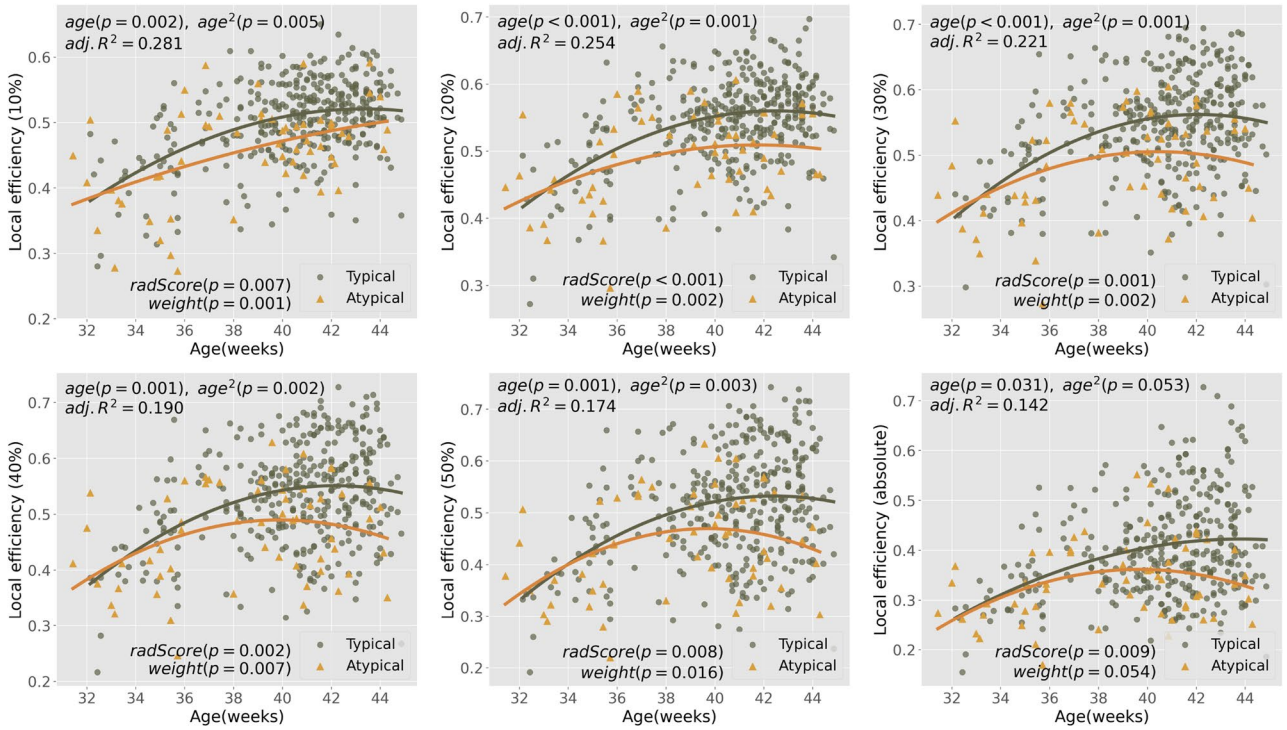

Fig. 3 Local efficiency values as a function of age as well as radScore differences across different thresholds. The plots show the regression line for local efficiency values from 31 to 45 postmenstrual weeks of age. The $adj.R^2$ values were determined using *age* and age^2 as predictors, and *weight* and *radScore* as other covariates

Table 2 Hub regions and their accordance indexes in UNC-CEDARS (Shi et al. 2018) atlas. The network hubs were identified as nodes with high degrees ($k >$ Mean + 1.5 SD; Mean = 66.64, SD = 23.24). See supplementary Table S1 for full results

Index	Region	Abbreviation	Degree(k)
2	Precentral gyrus left	PreCG-L	103
33	Middle frontal gyrus left	MFG-L	104
36	Middle frontal gyrus right	MFG-R	107
62	Superior frontal gyrus (medial) left	SFGmed-L	104
67	Superior frontal gyrus (medial) right	SFGmed-R	102
90	Anterior cingulate gyrus right	ACG-R	106
92	Middle cingulate gyrus left	MCG-L	103
95	Middle cingulate gyrus right	MCG-R	102
167	Precuneus right	PCUN-R	103
203	Middle temporal gyrus left	MTG-L	102
205	Middle temporal gyrus right	MTG-R	102

Moreover, significant differences in radScore ($p < 0.05$) were noted across the age range for the normalized rich-club coefficient of the functional connectomes.

Discussion

The current study investigated the topology of functional connectomes derived from rs-fMRI data during early development and explored the impact of age, weight, gender, and typical/atypical development on both global and local network metrics. To the modest knowledge of the researchers, this is the first study to apply network science to examine the development of functional connectomes using functional atlas parcellation during the neonatal period. Moreover, various thresholding approaches were employed to confirm the findings. Our results demonstrated that: (i) the brain network from 31 to 45 postmenstrual weeks displayed increases in global efficiency, local efficiency, small-worldness, and clustering coefficient and decreases in modularity and characteristic path length. The normalized rich-club coefficient showed a positive quadratic change related to the degree of premature birth (Figures 2-7); (ii) typical subjects showed higher values for global efficiency (Fig. 2), local efficiency (Fig. 3), normalized rich-club coefficient (Fig. 4), clustering coefficient (Fig. 5b), and lower values for characteristic path length (Fig. 5a) compared to atypical subjects; (iii) the network hubs were mainly situated in PreCG-L, MFG, SFGmed,

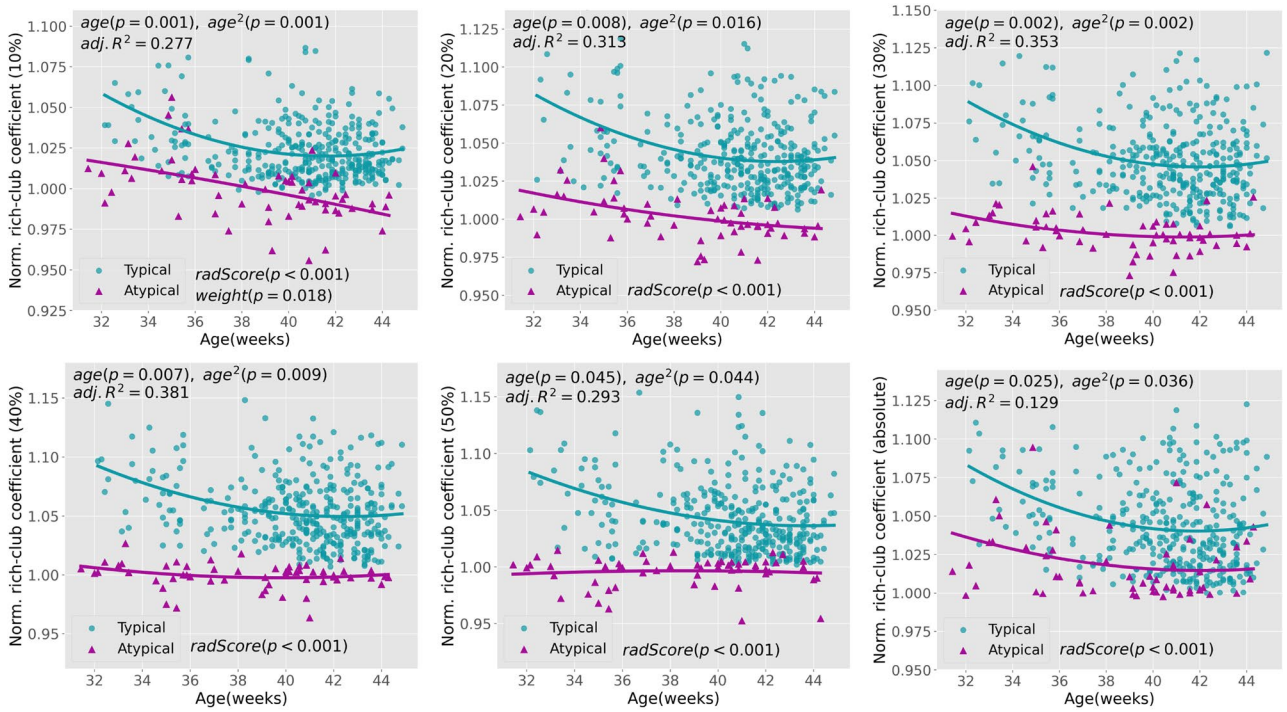

Fig. 4 Normalized rich-club coefficient values as a function of age as well as radScore differences across various thresholds. The plots illustrate the regression line for normalized rich-club coefficient values from 31 to 45 postmenstrual weeks of age. The *adj.*R^2 values for normalized rich-club coefficient across different thresholds, with the exception of the 10% density network, were determined using *age* and age^2 as predictors, and *radScore* as other covariates. For the 10% density network, the *adj.*R^2 value was calculated using *age* and age^2 as predictors, and *weight* and *radScore* as other covariates

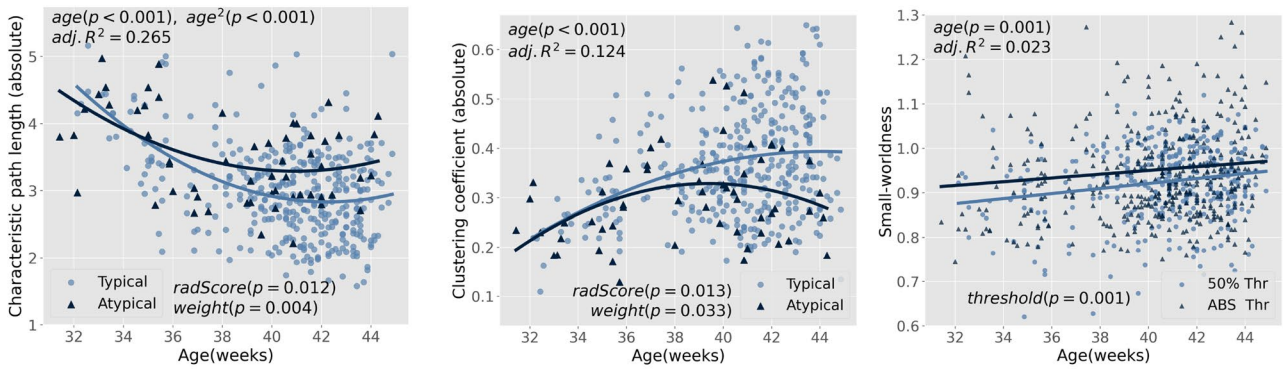

(a) Characteristic path length (b) Clustering coefficient (c) Small-worldness

Fig. 5 Age-related changes in the topological characteristics of the functional connectomes. The plots depict the regression line for **a** Characteristic path length, **b** Clustering coefficient, and **c** Small-worldness values observed between 31 and 45 postmenstrual weeks of age. The *adj.*R^2 values for characteristic path length and clustering coefficient were determined using *age* and age^2 as predictors, and *weight* and *radScore* as other covariates. The *adj.*R^2 value for the small-worldness was calculated using *age* as the predictor and *threshold* as the other covariate

ACG-R, MCG, PCUN-R, and MTG during the developmental period (Table 2); (iv) the network characteristics correlated with age, weight, and radiology score but not with gender factor. Although values across multiple thresholds were considered, the findings indicated significant gender differences in modularity (Fig. 7d) and normalized rich-club coefficient (Fig. 7c). Overall, significant topological changes were detected in human functional

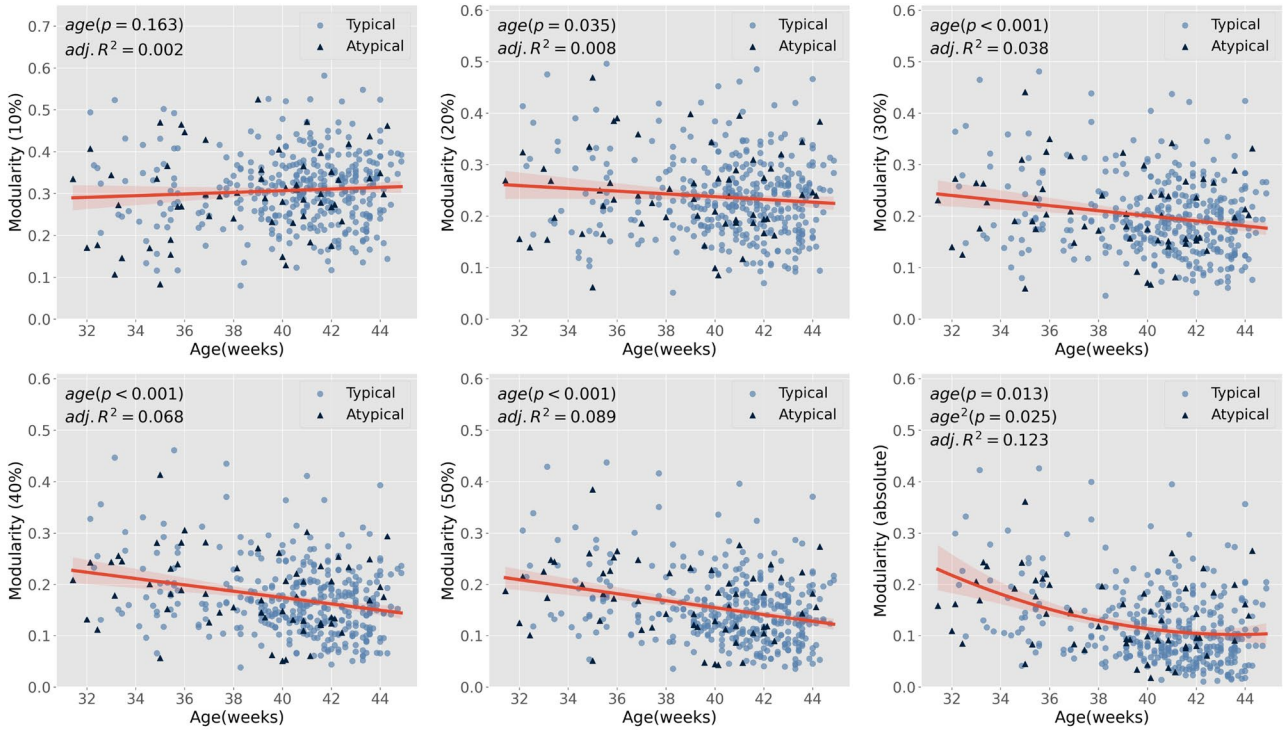

Fig. 6 Modularity values as a function of age across different thresholds. As there were no significant differences in radScore for modularity, the plots display a single regression line for all subjects, including both typical and atypical individuals. The *adj.*R^2 values for modularity across various thresholds, except for the absolute thresholding network, were determined using *age* as a predictor. For the absolute thresholding network, the *adj.*R^2 value was calculated using *age* and *age*^{2} as predictors

connectomes from 31 to 45 postmenstrual weeks, which could be influenced by neonatal age, weight, and radiology score.

The properties of brain networks are categorized according to how they relate to the processes of segregation and integration (Rubinov and Sporns 2010; Stam 2010; Bullmore and Bassett 2011). Topological segregation is the neuronal processing that occurs between spatially neighboring nodes via local connections that are relatively short in length, ensuring functional specialization. The local efficiency and average clustering coefficient of a network's nodes are the two quantitative measures for the networks' segregation capacity. The integration process, on the other hand, indicates the effectiveness of global information communication or the network's capability to integrate distributed information, and it is calculated by a network's global efficiency or characteristic path length (Rubinov and Sporns 2010; Stam 2010; Bullmore and Bassett 2011). In the present study, global efficiency significantly increased, while modularity and characteristic path length decreased in functional connectomes with age, indicating a progressively improved global information transfer effectiveness. Therefore, these findings show that the network integration process improves gradually with age. Furthermore, with an increase in the local efficiency and clustering coefficient during the developmental period, the connections became more locally clustered. This led to a growth in the network's local information transfer capability, fault tolerance capacity, and a high degree of network segregation (Rubinov and Sporns 2010; Stam 2010; Bullmore and Bassett 2011; Sporns 2013). Functional segregation enables distinct functional components or modules to engage in specialized processing, thereby enhancing the overall efficiency of the brain network (Sporns and Betzel 2016; Kline et al. 2021). Remarkably, the brain's segregation development displayed a sound concordance with developments in behaviors and cognitive abilities (Werner 1957; Johnson 2000; Sameroff 2010). As Werner's "orthogenetic principle" proposes, the behavior's increased differentiation and hierarchical organization happen in the processes of child development (Werner 1957; Sameroff 2010). The interactive specialization framework (Johnson 2000) auspicated that during maturation, the networks and the regions within them would become segregated and functionally specialized, leading to distinct behaviors and cognitive capacities.

The findings of several studies align with our results, demonstrating an increase in both global and local efficiency (Gao et al. 2011; Berchicci et al. 2015), as well as a decrease in modularity (Thomason et al. 2014) with age. In one-year-old infants, global and local efficiencies

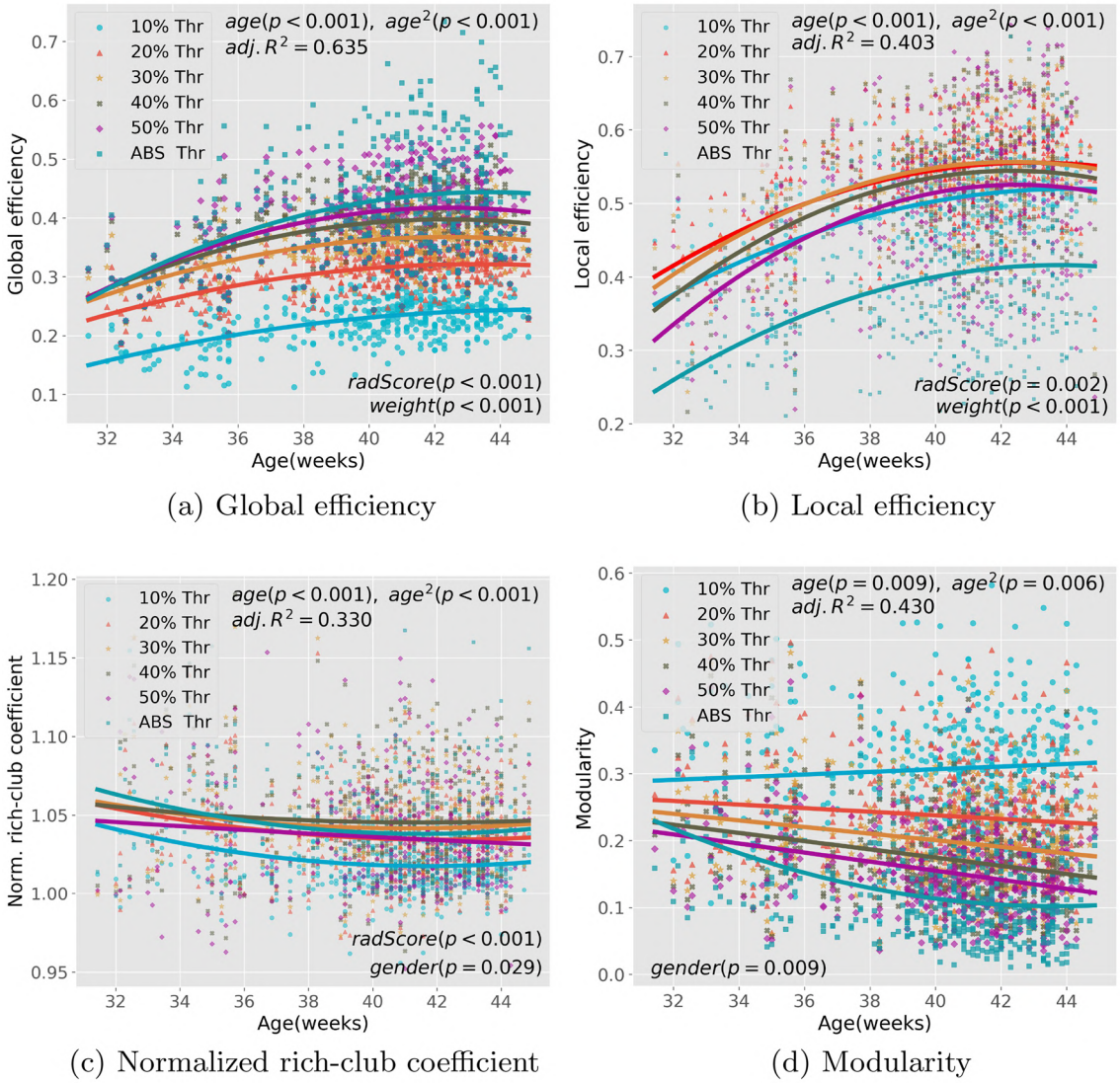

Fig. 7 Age-related changes in the topological characteristics of the functional connectomes across various thresholds. The plots illustrate the regression line for **a** Global efficiency, **b** Local efficiency, **c** Normalized rich-club coefficient, and **d** Modularity values between 31 and 45 postmenstrual weeks of age across all thresholds. The network properties show different values at different thresholds. Considering values across multiple thresholds, the findings indicated significant gender differences in normalized rich-club coefficient and modularity. The $adj.R^2$ values for global efficiency and local efficiency were determined using *age* and age^2 as predictors, and *weight*, *radScore*, and *threshold* as other covariates. Similarly, the $adj.R^2$ value for the normalized rich-club coefficient was obtained using *age* and age^2 as predictors, and *weight*, *gender*, *radScore*, and *threshold* as other covariates. Lastly, the $adj.R^2$ value for modularity was calculated using *age* and age^2 as predictors, and *weight*, *gender*, and *threshold* as other covariates

of functional connectomes increased compared to neonates but remained stable in the second year after birth (Gao et al. 2011). Long-distance links were primarily responsible for the increased global efficiency. Research on fetal fMRI discovered that the network integration process improves with age, demonstrated by a decrease in modularity and an increase in the strength of inter-module connections (Thomason et al. 2014). In one MEG investigation, the global and local efficiencies of the sensorimotor network both significantly increased after the first year of life (Berchicci et al. 2015). During the first few postnatal years, these changes indicate an improvement in the network integration and segregation processes. However, some studies yielded contradictory results. According to the EEG study (Toth et al. 2017), infants showed a shift toward a less centralized and more hierarchical network topology at the alpha- and theta-bands suggesting an improvement in network segregation. Additionally, an age-related increase in diameter, akin to the characteristic path length, was observed in the infants' brains, indicating a reduction in network integration (Toth

et al. 2017). Therefore, these findings are partly in line with those of the current study. Some differences in methodology, such as how thresholding approaches are selected or network nodes are defined, or the use of various functional brain imaging techniques may justify these discrepancies.

The other main finding of the current study was an increase in the functional specificity of neonatal brains from a network science standpoint. Similar to the study by Cao et al. (2017), a notable small-world topology was identified throughout the studied age range. Additionally, a positive age impact on small-worldness was detected indicating the appearance of functional segregation and integration patterns. In a complex network, the existence of an optimal balance between the integration and segregation of the small-world topology is necessary for having a fast information transfer and a high synchronizability (Watts and Strogatz 1998; Latora and Marchiori 2001). Indeed, neonatal functional networks can display an optimal balance between regional segregation and global integration of information transmission (Rubinov and Sporns 2010). Based on some recent studies, the small-world property is founded in the structural brain networks during the early stages of development (Tymofiyeva et al. 2013; Brown et al. 2014; Van Den Heuvel et al. 2015; Batalle et al. 2017). It exercises a negative age impact in the functional brain networks throughout childhood (Gozdas et al. 2019), while it remains unchanged in children as well as young adults (Wu et al. 2013). Therefore, the present study findings provide additional support for the previous findings revealing that the functional connectomes show prominent small-world structure during the neonatal period.

The presence of the hubs generally supports small-world networks. These high-central or high-degree nodes tend to interconnect densely and establish a rich-club architecture, forming the backbone for effective communication throughout the brain network (Van Den Heuvel and Sporns 2011). Studies on the functional hubs reveal that the hubs in prenatal and neonatal brain networks mainly exist in the primary sensorimotor, motor, auditory, and visual areas (Fransson et al. 2011; Gao et al. 2011; Asis-Cruz et al. 2015; van den Heuvel et al. 2018; Rajasilta et al. 2020). These results are in line with the present study findings shown in Table 2. The existence of hubs in the neonatal period shows that the functional connectomes are non-random in various areas and play diverse roles in the process of information communication. In line with Cao et al. (2017) study, we found that the rich-club architecture emerged at 31 PMW and developed in size with age. The normalized rich-club coefficient was detected with a U-shaped developmental trajectory. It shows that the normalized rich-club coefficient decreased until around 40 PMW and increased at an older age. It indicates that the functional hub distribution evolution keeps on across the dynamic local reconfigurations after birth. The hubs and rich-club organizations play major roles in the global transmission of information, albeit at the cost of comparatively high wiring and running expenses as well as attack resilience (Bullmore and Sporns 2012; Van Den Heuvel et al. 2012; Tomasi et al. 2013). It is worth noting that the impacts of prematurity on the later hub and rich-club distribution changes were not investigated in the present study, because the longitudinal rs-fMRI data of preterm-born and term-born infants were not available.

Limitations

The present study has some limitations. First, cross-sectional analyses are known to suffer from the potential confounding of between-subjects variability with aging effects. This means that the association between age, cognitive function, and network metrics cannot be fully investigated using this approach due to cross-sectional mediation (Lindenberger and Pötter 1998; Hofer and Sliwinski 2001; Raz and Lindenberger 2011). To address this issue, longitudinal studies should be carried out to investigate age-related changes and examine the correlation between brain metrics and cognitive performance.

The second limitation of this study is related to the relatively small sample size of atypical infants compared to the typical group, which could undermine the reliability of the findings for the former group. Future research endeavors should aim to generate more accurate estimates of cross-sectional trajectories by leveraging larger data samples to address this issue. Specifically, longitudinal investigations employing expansive sample sizes would be instrumental in providing a more comprehensive depiction of the early developmental path of the functional brain connectome.

Lastly, it is worth noting that the imaging system used for the dHCP study was designed specifically for neonatal imaging. While the custom head coil provides exceptional SNR on the cortical surface, this creates a bias toward sources that are located closer to the surface (Hughes et al. 2017). This bias is further amplified by the use of highly accelerated multiband EPI (Fitzgibbon et al. 2020). Furthermore, despite the use of advanced distortion correction techniques in the dHCP pipeline (Fitzgibbon et al. 2020), some signal loss may occur due to bone/tissue and air/tissue interfaces. Moreover, motion can affect the quality of the fMRI signal (Power et al. 2012; Satterthwaite et al. 2012), and the observation that term-born neonates exhibited greater motion compared to preterm-born neonates raises the possibility that motion artifacts may have influenced the findings. Nonetheless, the dHCP pipeline includes several measures to counteract the impact of motion and physiological confounds, thereby reducing data loss. Furthermore, we eliminated infants displaying

excessive motion during the analyses. However, we cannot fully consider any inherent distinctions in BOLD signal between term-born and preterm-born babies that could be attributed to cerebrovascular factors (Bouyssi-Kobar et al. 2018). Additional approaches, such as EEG, could potentially aid in addressing this issue (Arichi et al. 2017).

Conclusion

The functional brain network topology in early development and the effects of age, weight, gender, and typical and atypical development on the brain network organization were examined in the present study. Significant age, weight, and radiology score-related changes were found in the developmental trajectories, showing various rates of maturation in the typical and atypical subjects. They show an increase in network segregation and integration processes in the neonatal period. The dynamics of the functional brain network regionally and globally were presented in this study providing a new insight into understanding the brain maturation of the functional connectome. It would help detect the anomalies associated with neurodevelopmental disorders. In this study, the functional brain changes were studied without carrying out structural analysis. The latter could provide a wider perspective on how the brain changes with age by noting the structural discrepancies and their relationships with the functional findings. Studies including this association might improve our understanding of the physiological mechanisms behind age-related alterations. More research is required to determine the role of the structural connectome in functional connectivity formation and regulation.

Supplementary Information The online version contains supplementary material available at https://doi.org/10.1007/s00429-023-02681-4.

Acknowledgements Data were provided by the developing Human Connectome Project, KCL-Imperial-Oxford Consortium funded by the European Research Council under the European Union Seventh Framework Programme (FP/2007-2013) / ERC Grant Agreement no. [319456]. We are grateful to the families who generously supported this trial. This work was partially supported by the Institute for Research in Fundamental Science (IPM) of Iran under the grant No. CS1402-4-162.

Author contributions Both authors contributed to the study conception and design. Material preparation, data collection was performed by RN and MS. RN implemented the computer code and supporting algorithms and analyzed the data. RN wrote the manuscript and MS commented on previous versions of the manuscript. Both authors read and approved the final manuscript.

Funding This work was partially supported by the Institute for Research in Fundamental Science (IPM) of Iran under the grant No. CS1402-4-162.

Data availability The dHCP is an open-access project. The data that support the findings of this study are openly available at the following URL: http://www.developingconnectome.org.

Declarations

Conflict of interest The authors have no relevant financial or non-financial interests to disclose.

References

Abraham A, Pedregosa F, Eickenberg M et al (2014) Machine learning for neuroimaging with scikit-learn. Front Neuroinformatics 8:14. https://doi.org/10.3389/fninf.2014.00014

Alstott J, Panzarasa P, Rubinov M et al (2014) A unifying framework for measuring weighted rich clubs. Sci Rep 4(1):1–6. https://doi.org/10.1038/srep07258

Arichi T, Whitehead K, Barone G et al (2017) Localization of spontaneous bursting neuronal activity in the preterm human brain with simultaneous eeg-fmri. elife 6:e27,814. https://doi.org/10.7554/eLife.27814

Asis-Cruz D, Bouyssi-Kobar M, Evangelou I et al (2015) Functional properties of resting state networks in healthy full-term newborns. Sci Rep 5(1):1–15. https://doi.org/10.1038/srep17755

Avants BB, Tustison N, Song G et al (2009) Advanced normalization tools (ants). Insight J 2(365):1–35

Batalle D, Hughes EJ, Zhang H et al (2017) Early development of structural networks and the impact of prematurity on brain connectivity. Neuroimage 149:379–392. https://doi.org/10.1016/j.neuroimage.2017.01.065

Berchicci M, Tamburro G, Comani S (2015) The intrahemispheric functional properties of the developing sensorimotor cortex are influenced by maturation. Front Hum Neurosci 9:39. https://doi.org/10.3389/fnhum.2015.00039

Boeken OJ, Cieslik EC, Langner R et al (2022) Characterizing functional modules in the human thalamus: coactivation-based parcellation and systems-level functional decoding. Brain Struct Func. https://doi.org/10.1007/s00429-022-02603-w

Bouyssi-Kobar M, Murnick J, Brossard-Racine M et al (2018) Altered cerebral perfusion in infants born preterm compared with infants born full term. J Pediatr 193:54–61. https://doi.org/10.1016/j.jpeds.2017.09.083

Bozek J, Makropoulos A, Schuh A et al (2018) Construction of a neonatal cortical surface atlas using multimodal surface matching in the developing human connectome project. Neuroimage 179:11–29. https://doi.org/10.1016/j.neuroimage.2018.06.018

Brown CJ, Miller SP, Booth BG et al (2014) Structural network analysis of brain development in young preterm neonates. Neuroimage 101:667–680. https://doi.org/10.1016/j.neuroimage.2014.07.030

Bullmore ET, Bassett DS (2011) Brain graphs: graphical models of the human brain connectome. Ann Rev Clin Psychol 7:113–140. https://doi.org/10.1146/annurev-clinpsy-040510-143934

Bullmore E, Sporns O (2009) Complex brain networks: graph theoretical analysis of structural and functional systems. Nat Rev Neurosci 10(3):186–198. https://doi.org/10.1038/nrn2575

Bullmore E, Sporns O (2012) The economy of brain network organization. Nat Rev Neurosci 13(5):336–349. https://doi.org/10.1038/nrn3214

Cao M, He Y, Dai Z et al (2017) Early development of functional network segregation revealed by connectomic analysis of the preterm human brain. Cereb Cortex 27(3):1949–1963. https://doi.org/10.1093/cercor/bhw038

Cao M, Huang H, He Y (2017) Developmental connectomics from infancy through early childhood. Trends Neurosci 40(8):494–506. https://doi.org/10.1016/j.tins.2017.06.003

Cao H, McEwen SC, Forsyth JK et al (2019) Toward leveraging human connectomic data in large consortia: generalizability of fmri-based brain graphs across sites, sessions, and paradigms. Cereb Cortex 29(3):1263–1279. https://doi.org/10.1093/cercor/bhy032

Centeno EGZ, Moreni G, Vriend C et al (2022) A hands-on tutorial on network and topological neuroscience. Brain Struct Funct 227(3):741–762. https://doi.org/10.1007/s00429-021-02435-0

Chen Z, Daniel E, Chen BT (2021) Phase fmri defines brain resting-state functional hubs within central and posterior regions. Brain Struct Funct 226(6):1925–1941. https://doi.org/10.1007/s00429-021-02301-z

Cohen JR, D'Esposito M (2016) The segregation and integration of distinct brain networks and their relationship to cognition. J Neurosci 36(48):12,083-12,094. https://doi.org/10.1523/JNEUROSCI.2965-15.2016

Cordero-Grande L, Hughes EJ, Hutter J et al (2018) Three-dimensional motion corrected sensitivity encoding reconstruction for multi-shot multi-slice mri: application to neonatal brain imaging. Magn Reson Med 79(3):1365–1376. https://doi.org/10.1002/mrm.26796

Craddock RC, James GA, Holtzheimer PE III et al (2012) A whole brain fmri atlas generated via spatially constrained spectral clustering. Hum Brain Mapp 33(8):1914–1928. https://doi.org/10.1002/hbm.21333

Cusack R, Linke AC, Zubiaurre-Elorza L, et al (2017) Differences in the spatial and temporal patterns of head motion during mri of adults and infants. bioRxiv 114447. https://doi.org/10.1101/114447

developing HCP consortium KIO (2021) Developing human connectome project (dhcp). http://www.developingconnectome.org, accessed: 2022-05-25

Emerson RW, Gao W, Lin W (2016) Longitudinal study of the emerging functional connectivity asymmetry of primary language regions during infancy. J Neurosci 36(42):10,883-10,892. https://doi.org/10.1523/JNEUROSCI.3980-15.2016

Fitzgibbon SP, Harrison SJ, Jenkinson M et al (2020) The developing human connectome project (dhcp) automated resting-state functional processing framework for newborn infants. Neuroimage 223(117):303. https://doi.org/10.1016/j.neuroimage.2020.117303

Fransson P, Åden U, Blennow M et al (2011) The functional architecture of the infant brain as revealed by resting-state fmri. Cereb Cortex 21(1):145–154. https://doi.org/10.1093/cercor/bhq071

Gao W, Gilmore JH, Giovanello KS et al (2011) Temporal and spatial evolution of brain network topology during the first two years of life. PloS one 6(9):e25,278. https://doi.org/10.1371/journal.pone.0025278

Gao W, Alcauter S, Smith JK et al (2015) Development of human brain cortical network architecture during infancy. Brain Struct Funct 220(2):1173–1186. https://doi.org/10.1007/s00429-014-0710-3

Garrison KA, Scheinost D, Finn ES et al (2015) The (in) stability of functional brain network measures across thresholds. Neuroimage 118:651–661. https://doi.org/10.1016/j.neuroimage.2015.05.046

Gilmore JH, Knickmeyer RC, Gao W (2018) Imaging structural and functional brain development in early childhood. Nature Rev Neurosci 19(3):123–137. https://doi.org/10.1038/nrn.2018.1

Gorgolewski KJ, Auer T, Calhoun VD et al (2016) The brain imaging data structure, a format for organizing and describing outputs of neuroimaging experiments. Sci data 3(1):1–9. https://doi.org/10.1038/sdata.2016.44

Gozdas E, Holland SK, Altaye M et al (2019) Developmental changes in functional brain networks from birth through adolescence. Human Brain Mapp 40(5):1434–1444. https://doi.org/10.1002/hbm.24457

Hazlett HC, Gu H, Munsell BC et al (2017) Early brain development in infants at high risk for autism spectrum disorder. Nature 542(7641):348–351. https://doi.org/10.1038/nature21369

Hofer SM, Sliwinski MJ (2001) Understanding ageing. Gerontology 47(6):341–352. https://doi.org/10.1159/000052825

Howell AL, Osher DE, Li J et al (2020) The intrinsic neonatal hippocampal network: rsfmri findings. J Neurophysiol 124(5):1458–1468. https://doi.org/10.1152/jn.00362.2020

Hughes EJ, Winchman T, Padormo F et al (2017) A dedicated neonatal brain imaging system. Magn Reson Med 78(2):794–804. https://doi.org/10.1002/mrm.26462

Huttenlocher PR et al (1979) Synaptic density in human frontal cortex-developmental changes and effects of aging. Brain Res 163(2):195–205. https://doi.org/10.1016/0006-8993(79)90349-4

Huttenlocher PR, Dabholkar AS (1997) Regional differences in synaptogenesis in human cerebral cortex. J Comp Neurol 387(2):167–178. https://doi.org/10.1002/(SICI)1096-9861(19971020)387:2<167::AID-CNE1>3.0.CO;2-Z

Jenkinson M, Beckmann CF, Behrens TE et al (2012) Fsl. Neuroimage 62(2):782–790. https://doi.org/10.1016/j.neuroimage.2011.09.015

John M, Ikuta T, Ferbinteanu J (2017) Graph analysis of structural brain networks in alzheimer's disease: beyond small world properties. Brain Struct Funct 222(2):923–942. https://doi.org/10.1007/s00429-016-1255-4

Johnson MH (2000) Functional brain development in infants: elements of an interactive specialization framework. Child Dev 71(1):75–81. https://doi.org/10.1111/1467-8624.00120

Kelly C, Biswal BB, Craddock RC et al (2012) Characterizing variation in the functional connectome: promise and pitfalls. Trends Cogn Sci 16(3):181–188. https://doi.org/10.1016/j.tics.2012.02.001

Kim DJ, Min BK (2020) Rich-club in the brain's macrostructure: insights from graph theoretical analysis. Comput Struct Biotechnol J 18:1761–1773. https://doi.org/10.1016/j.csbj.2020.06.039

Kline JE, Illapani VSP, Li H et al (2021) Diffuse white matter abnormality in very preterm infants at term reflects reduced brain network efficiency. NeuroImage: Clin 31:102,739. https://doi.org/10.1016/j.nicl.2021.102739

Knickmeyer RC, Gouttard S, Kang C et al (2008) A structural mri study of human brain development from birth to 2 years. J Neurosci 28(47):12,176-12,182. https://doi.org/10.1523/JNEUROSCI.3479-08.2008

Kostović I, Sedmak G, Judaš M (2019) Neural histology and neurogenesis of the human fetal and infant brain. Neuroimage 188:743–773. https://doi.org/10.1016/j.neuroimage.2018.12.043

Latora V, Marchiori M (2001) Efficient behavior of small-world networks. Phys Rev Lett 87(19):198,701. https://doi.org/10.1103/PhysRevLett.87.198701

Li G, Wang L, Yap PT et al (2019) Computational neuroanatomy of baby brains: a review. NeuroImage 185:906–925. https://doi.org/10.1016/j.neuroimage.2018.03.042

Lindenberger U, Pötter U (1998) The complex nature of unique and shared effects in hierarchical linear regression: implications for developmental psychology. Psychol Methods 3(2):218. https://doi.org/10.1037/1082-989X.3.2.218

Makropoulos A, Gousias IS, Ledig C et al (2014) Automatic whole brain mri segmentation of the developing neonatal brain. IEEE Trans Med Imaging 33(9):1818–1831. https://doi.org/10.1109/TMI.2014.2322280

Makropoulos A, Robinson EC, Schuh A et al (2018) The developing human connectome project: a minimal processing pipeline for

neonatal cortical surface reconstruction. Neuroimage 173:88–112. https://doi.org/10.1016/j.neuroimage.2018.01.054
Malik S (2015) Optimized amplitude modulated multi-band rf pulses. In: Proceedings of international society for magnetic resonance in medicine, p 2398, 10.1002/mrm.26610
Marín O (2016) Developmental timing and critical windows for the treatment of psychiatric disorders. Nat Medicine 22(11):1229–1238. https://doi.org/10.1038/nm.4225
Markett S, Montag C, Heeren B et al (2016) Voxelwise eigenvector centrality mapping of the human functional connectome reveals an influence of the catechol-o-methyltransferase val158met polymorphism on the default mode and somatomotor network. Brain Struct Funct 221:2755–2765. https://doi.org/10.1007/s00429-015-1069-9
McGrath H, Zaveri HP, Collins E et al (2022) High-resolution cortical parcellation based on conserved brain landmarks for localization of multimodal data to the nearest centimeter. Sci Rep 12(1):18,778. https://doi.org/10.1038/s41598-022-21543-3
Mijalkov M, Veréb D, Jamialahmadi O et al (2023) Sex differences in multilayer functional network topology over the course of aging in 37543 UK biobank participants. Network Neurosci 7(1):351–376. https://doi.org/10.1162/netn_a_00286
Miller DJ, Duka T, Stimpson CD et al (2012) Prolonged myelination in human neocortical evolution. Proc Natl Acad Sci 109(41):16,480-16,485. https://doi.org/10.1073/pnas.1117943109
Mongerson CR, Jennings RW, Borsook D et al (2017) Resting-state functional connectivity in the infant brain: methods, pitfalls, and potentiality. Front Pediatr 5:159. https://doi.org/10.3389/fped.2017.00159
Neudorf J, Kress S, Borowsky R (2022) Structure can predict function in the human brain: a graph neural network deep learning model of functional connectivity and centrality based on structural connectivity. Brain Struct Funct 227(1):331–343. https://doi.org/10.1007/s00429-021-02403-8
Newman ME (2006) Modularity and community structure in networks. Proc Natl Acad Sci 103(23):8577–8582. https://doi.org/10.1073/pnas.0601602103
Onoda K, Yamaguchi S (2013) Small-worldness and modularity of the resting-state functional brain network decrease with aging. Neurosci Lett 556:104–108. https://doi.org/10.1016/j.neulet.2013.10.023
Opsahl T, Colizza V, Panzarasa P et al (2008) Prominence and control: the weighted rich-club effect. Phys Rev Lett 101(16):168,702. https://doi.org/10.1103/PhysRevLett.101.168702
Päeske L, Hinrikus H, Lass J et al (2020) Negative correlation between functional connectivity and small-worldness in the alpha frequency band of a healthy brain. Front Physiol 11:910. https://doi.org/10.3389/fphys.2020.00910
Power JD, Barnes KA, Snyder AZ et al (2012) Corrigendum to "spurious but systematic correlations in functional connectivity mri networks arise from subject motion''. NeuroImage 63(2):999. https://doi.org/10.1016/j.neuroimage.2012.01.069
Price A, Cordero-Grande L, Malik S, et al (2015) Accelerated neonatal fmri using multiband epi. In: Proceedings of the 23rd Annual Meeting of ISMRM, Toronto, Canada, p 3911
Rajasilta O, Tuulari JJ, Björnsdotter M et al (2020) Resting-state networks of the neonate brain identified using independent component analysis. Dev Neurobiol 80(3–4):111–125. https://doi.org/10.1002/dneu.22742
Raz N, Lindenberger U (2011) Only time will tell: cross-sectional studies offer no solution to the age-brain-cognition triangle: Comment on salthouse (2011). Psychol Bull 137(5):790–795. https://doi.org/10.1037/a0024503
Rubinov M, Sporns O (2010) Complex network measures of brain connectivity: uses and interpretations. Neuroimage 52(3):1059–1069. https://doi.org/10.1016/j.neuroimage.2009.10.003
Salehi M, Rabiee HR, Jalili M (2010) Motif structure and cooperation in real-world complex networks. Physica A: Stat Mech Appl 389(23):5521–5529. https://doi.org/10.1016/j.physa.2010.08.001
Salimi-Khorshidi G, Douaud G, Beckmann CF et al (2014) Automatic denoising of functional mri data: combining independent component analysis and hierarchical fusion of classifiers. Neuroimage 90:449–468. https://doi.org/10.1016/j.neuroimage.2013.11.046
Sameroff A (2010) A unified theory of development: a dialectic integration of nature and nurture. Child Dev 81(1):6–22. https://doi.org/10.1111/j.1467-8624.2009.01378.x
Satterthwaite TD, Wolf DH, Loughead J et al (2012) Impact of in-scanner head motion on multiple measures of functional connectivity: relevance for studies of neurodevelopment in youth. Neuroimage 60(1):623–632. https://doi.org/10.1016/j.neuroimage.2011.12.063
Seabold S, Perktold J (2010) Statsmodels: Econometric and statistical modeling with python. In: Proceedings of the 9th python in science conference, Austin, TX, p 61
Serag A, Aljabar P, Ball G et al (2012) Construction of a consistent high-definition spatio-temporal atlas of the developing brain using adaptive kernel regression. Neuroimage 59(3):2255–2265. https://doi.org/10.1016/j.neuroimage.2011.09.062
Shi F, Salzwedel AP, Lin W et al (2018) Functional brain parcellations of the infant brain and the associated developmental trends. Cereb Cortex 28(4):1358–1368. https://doi.org/10.1093/cercor/bhx062
Smith SM (2002) Fast robust automated brain extraction. Hum Brain Mapp 17(3):143–155. https://doi.org/10.1002/hbm.10062
Smith SM, Jenkinson M, Woolrich MW et al (2004) Advances in functional and structural mr image analysis and implementation as fsl. Neuroimage 23:S208–S219. https://doi.org/10.1016/j.neuroimage.2004.07.051
Smith DV, Utevsky AV, Bland AR et al (2014) Characterizing individual differences in functional connectivity using dual-regression and seed-based approaches. Neuroimage 95:1–12. https://doi.org/10.1016/j.neuroimage.2014.03.042
Smyser CD, Snyder AZ, Shimony JS et al (2016) Resting-state network complexity and magnitude are reduced in prematurely born infants. Cereb Cortex 26(1):322–333. https://doi.org/10.1093/cercor/bhu251
Sporns O (2013) Network attributes for segregation and integration in the human brain. Curr Opin Neurobiol 23(2):162–171. https://doi.org/10.1016/j.conb.2012.11.015
Sporns O, Betzel RF (2016) Modular brain networks. Ann Rev Psychol 67:613–640. https://doi.org/10.1146/annurev-psych-122414-033634
Stam C (2010) Characterization of anatomical and functional connectivity in the brain: a complex networks perspective. Int J Psychophysiol 77(3):186–194. https://doi.org/10.1016/j.ijpsycho.2010.06.024
Thomason ME, Brown JA, Dassanayake MT et al (2014) Intrinsic functional brain architecture derived from graph theoretical analysis in the human fetus. PLoS one 9(5):e94,423. https://doi.org/10.1371/journal.pone.0094423
Thomason ME, Grove LE, Lozon TA Jr et al (2015) Age-related increases in long-range connectivity in fetal functional neural connectivity networks in utero. Dev Cogn Neurosci 11:96–104. https://doi.org/10.1016/j.dcn.2014.09.001
Tomasi D, Wang GJ, Volkow ND (2013) Energetic cost of brain functional connectivity. Proc Natl Acad Sci 110(33):13,642-13,647. https://doi.org/10.1073/pnas.1303346110

Toth B, Urban G, Haden GP et al (2017) Large-scale network organization of eeg functional connectivity in newborn infants. Hum Brain Mapp 38(8):4019–4033. https://doi.org/10.1002/hbm.23645

Tustison NJ, Avants BB, Cook PA et al (2010) N4itk: improved n3 bias correction. IEEE Trans Med Imaging 29(6):1310–1320. https://doi.org/10.1109/TMI.2010.2046908

Tymofiyeva O, Hess CP, Ziv E et al (2013) A dti-based template-free cortical connectome study of brain maturation. PloS one 8(5):e63,310. https://doi.org/10.1371/journal.pone.0063310

Van Den Heuvel MP, Sporns O (2011) Rich-club organization of the human connectome. J Neurosci 31(44):15,775-15,786. https://doi.org/10.1523/JNEUROSCI.3539-11.2011

van den Heuvel MP, Sporns O (2013) Network hubs in the human brain. Trends Cogn Sci 17(12):683–696. https://doi.org/10.1016/j.tics.2013.09.012

Van Den Heuvel MP, Kahn RS, Goñi J et al (2012) High-cost, high-capacity backbone for global brain communication. Proc Natl Acad Sci 109(28):11,372-11,377. https://doi.org/10.1073/pnas.1203593109

Van Den Heuvel MP, Kersbergen KJ, De Reus MA et al (2015) The neonatal connectome during preterm brain development. Cereb Cortex 25(9):3000–3013. https://doi.org/10.1093/cercor/bhu095

van den Heuvel MI, Turk E, Manning JH et al (2018) Hubs in the human fetal brain network. Dev Cogn Neurosci 30:108–115. https://doi.org/10.1016/j.dcn.2018.02.001

Watts DJ, Strogatz SH (1998) Collective dynamics of 'small-world'networks. Nature 393(6684):440–442. https://doi.org/10.1038/30918

Werner H (1957) The concept of development from a comparative and organismic point of view. University of Minnesota Press Minneapolis

Wu K, Taki Y, Sato K et al (2013) Topological organization of functional brain networks in healthy children: differences in relation to age, sex, and intelligence. PloS one 8(2):e55,347. https://doi.org/10.1371/journal.pone.0055347

Yakovlev P (1967) The myelogenetic cycles of regional maturation of the brain. Regional development of the brain in early life pp 3–70

Zhao T, Xu Y, He Y (2019) Graph theoretical modeling of baby brain networks. NeuroImage 185:711–727. https://doi.org/10.1016/j.neuroimage.2018.06.038

Zhao S, Wang G, Yan T et al (2021) Sex differences in anatomical rich-club and structural-functional coupling in the human brain network. Cereb Cortex 31(4):1987–1997. https://doi.org/10.1093/cercor/bhaa335